THE JOURNAL OF BIOLOGICAL CHEMISTRY VOL. 286, NO. 11, pp. 9216–9224, March 18, 2011

Identification of Two Major Conformational Aquaporin-4 Epitopes for Neuromyelitis Optica Autoantibody Binding*[S]

Received for publication, March 12, 2010, and in revised form, December 16, 2010 Published, JBC Papers in Press, January 6, 2011, DOI 10.1074/jbc.M110.123000

Francesco Pisani[‡], Mauro Mastrototaro[‡], Andrea Rossi[‡], Grazia Paola Nicchia[‡], Carla Tortorella[§], Maddalena Ruggieri[§], Maria Trojano[§], Antonio Frigeri[‡1], and Maria Svelto[‡]

From the [‡]Department of General and Environmental Physiology, Centre of Excellence in Comparative Genomics, and [§]Department of Neurological and Psychiatric Sciences, University of Bari, I-70126 Bari, Italy

Neuromyelitis optica (NMO) is an autoimmune demyelinating disease characterized by the presence of anti-aquaporin-4 (AQP4) antibodies in the patient sera. We recently reported that these autoantibodies are able to bind AQP4 when organized in the supramolecular structure called the orthogonal array of particles (OAP). To map the antigenic determinants, we produced a series of AQP4 mutants based on multiple alignment sequence analysis between AQP4 and other OAP-forming AQPs. Mutations were introduced in the three extracellular loops (A, C, and E), and the binding capacity of NMO sera was tested on AQP4 mutants. Results indicate that one group of sera was able to recognize a limited portion of loop C containing the amino acid sequence ^{146}GVT(T/M)V^{150}. A second group of sera was characterized by a predominant role of loop A. Deletion of four AQP4-specific amino acids (^{61}G(S/T)E(N/K)^{64}) in loop A substantially affected the binding of this group of sera. However, the binding capacity was further reduced when amino acids in loop A were mutated together with those in loop E or when those in loop C were mutated in combination with loop E. Finally, a series of AQP0 mutants were produced in which the extracellular loops were progressively changed to make them identical to AQP4. Results showed that none of the mutants was able to reproduce in AQP0 the NMO-IgG epitopes, indicating that the extracellular loop sequence by itself was not sufficient to determine the rearrangement required to create the epitopes. Although our data highlight the complexity of the disease, this study identifies key immunodominant epitopes and provides direct evidence that the transition from AQP4 tetramers to AQP4-OAPs involves conformational changes of the extracellular loops.

NMO[2] is a devastating autoimmune demyelinating disease, affecting primarily young women, and is associated with NMO-IgG antibodies detectable in the patient serum (1–6). Immunofluorescence using AQP4 null mice and AQP4-transfected cells (2) has amply demonstrated that the target of these autoantibodies is aquaporin-4 (AQP4), a water channel protein abundantly expressed in astrocyte end-foot near capillaries (7, 8). Autoantibodies against AQP4 (IgG) are found in about 75% of NMO patients, together with other autoantibodies for other proteins, including anti-myelin oligodendrocyte glycoprotein, anti-myelin basic protein, anti-S100 calcium-binding protein B (S100β), anti-cleavage polyadenylation specificity factor (CPSF-73), and anti-RING finger protein 141 (RNF-141) (2, 9–12). These other autoantibodies bind extra- or intracellular antigens liberated from dead cells and do not seem to have a pathogenic role in the NMO pathology (13). Anti-AQP4 IgG may act through the activation of multiple potentially neuropathogenic mechanisms contributing to injury to astrocytes and to the breakdown of the blood-brain barrier. These mechanisms include AQP4 internalization, an alteration of water and glutamate homeostasis, activation of antibody-dependent, cell-mediated cytotoxicity, and complement activation (14–17). The exact causes of the NMO pathogenesis are still unknown, but many hypotheses have been advanced. Bacterial or viral infections are believed to damage AQP4-expressing tissues and subsequently activate the autoimmune disease or that infection and autoimmunity may damage the blood-brain barrier and allow B and T cells to access the central nervous system (CNS).

One of the most intriguing questions regarding the pathogenesis of NMO is as follows. Why aren't all the AQP4-expressing tissues damaged in the NMO? Only the optic nerves, the spinal cord, and to a lesser extent the brain are mostly affected. The answer might lie in the molecular structure of the NMO-IgG epitope whose identification might lead to new insight into the pathogenic mechanism of the NMO IgG and contribute to the development of a specific therapy.

Until now, there are very few studies on this topic. A computational study predicts a conformational B cell epitope targeting the exposed AQP4 extracellular loops (13). The recent human AQP4 crystal structure (18) confirms this prediction and indicates that the flexibility of loop C is the most important structural characteristic of AQP4 that could have an important role in the NMO phatogenesis.

We have recently shown that the NMO-IgG selectively recognizes AQP4 only when organized in the plasma membrane to form supramolecular structures of AQP4 aggregates, called orthogonal arrays of particles (OAPs). NMO-IgGs are able to bind cells transfected with the OAP-forming M23 isoform of AQP4 but do not bind cells expressing only the M1 isoform, which is unable to form OAPs by itself (19, 20). Interestingly, NMO-IgGs are not able to bind the other two known OAP-

* This work was supported by the Apulia Region Grant Progetto Strategico APQ Ricerca PS124 (Neurobiotech) and Rete Nazionale di Proteomica Project RBRN07BMCT_009.

[S] The on-line version of this article (available at http://www.jbc.org) contains supplemental Figs. 1 and 2.

[1] To whom correspondence should be addressed. Tel.: 39-080-5443335; Fax: 39-080-5443388; E-mail: a.frigeri@biologia.uniba.it.

[2] The abbreviations used are: NMO, neuromyelitis optica; AQP4, aquaporin-4; OAP, orthogonal array of particle; BisTris, 2-[bis(2-hydroxyethyl)amino]-2-(hydroxymethyl)propane-1,3-diol; BN, blue native.

forming AQPs such as the lens-aquaporin 0 (AQP0) and the insect AQPcic (19, 21), indicating that the epitope for NMO-IgG is specific for AQP4-OAPs.

The aim of this study was to evaluate the molecular structure of the NMO-IgG epitope by generating a series of AQP4 mutants based on multiple alignment sequence analysis between AQP4 and other OAPs forming AQPs (AQP0 and AQPcic). Eleven NMO IgG sera were tested for their capability to bind these mutants. These sera recognized both human and rat AQP4.

EXPERIMENTAL PROCEDURES

Cell Cultures—HeLa cell line was grown in Dulbecco's high glucose medium with 10% fetal bovine serum and penicillin/streptomycin added (Invitrogen). To perform the transfection experiments, the cells were plated at 90–95% confluence.

Primary Amino Acid Sequence Multiple Alignment Analysis—The multiple alignment analysis of AQP0 and AQPcic and human, rat, and mouse AQP4 primary amino acid sequences has been performed using the ClustalW EBI tool. All the sequences were obtained from NCBI, Entrez Gene, Reference Sequences.

Site-directed Mutagenesis and Transfection of HeLa Cells—All the AQP4-M23 mutants, containing the mutations described in the Table 1, were obtained with a site-specific mutagenesis approach using QuikChange II site-directed mutagenesis kit (Stratagene) in according with manual instruction. Briefly, the AQP4-M23 isoforms (rat and human) were cloned into pcDNA3.1 (Invitrogen) and used as template in a long high fidelity PCR performed with *Pfu*Ultra® high fidelity DNA polymerase. The site-specific mutant primers were designed using the web-based QuikChange® primer design program from Stratagene available on line.

To obtain AQP0 mutants, human AQP0 CDS was cloned into a pTarget vector (Promega). Mutagenesis of AQP0 was done to replace all unmatched residues between APQ0 and human AQP4 in the extracellular loops (blue highlighted in the AQP0 sequence in supplemental Fig. 2). The mutants were named as follows (the AQP4 sequence is underlined): AQP0 loop A containing AQP4 loop A (GGTEKPLV); AQP0 loop C(a) containing part of the AQP4 loop C sequence (TPPSVVGGL-GVTMVHPAVSV); AQP0 loop C(b) containing the remaining part of the AQP4 loop C (TPPAVRGNLALNTLHGNLTA); AQP0 loop C(a+b) containing all the AQP4 loop C sequence (TPPSVVGGLGVTMVGNLTA); and AQP0 loop E containing the AQP4 loopE sequence (GNWENH). The other mutants we have generated are indicated in Table 3. The mutant plasmid DNAs (see Tables 1 and 3) were used for HeLa cell transfection experiments using Lipofectamine 2000 reagent (Invitrogen) according to the manufacturer's instructions.

GFP (N-terminal)-AQP4 and mCherry (C-terminal)—AQP4-M23 CDS was cloned into the pcDNA3.1 N-terminal GFP (Invitrogen) and the pmCherry-N1 (Clontech), according to the manufacturer's instructions, to obtain the AQP4-M23 isoform with an N-terminal GFP tag (GFP-M23) or with a C-terminal mCherry tag (M23-mCherry), respectively.

Antibodies and Patient Sera—Anti-AQP4 antibodies were from Santa Cruz Biotechnology (goat polyclonal IgG), diluted 1:300 and 1:500 for immunofluorescence and immunoblotting analysis, respectively. Anti-human AQP0 rabbit serum was purchased from Alpha Diagnostics and was diluted 1:500 for immunofluorescence analysis. NMO sera were employed at a dilution of 1:200 for immunofluorescence analysis.

The secondary antibody utilized for immunoblotting analysis was a donkey anti-goat IgG peroxidase conjugated from Santa Cruz Biotechnology at dilution of 1:10,000, and for immunofluorescence analysis, it was a donkey anti-goat or goat anti-human Alexa 488-conjugate, both at dilution of 1:1000.

Immunofluorescence Analysis—Transfected HeLa cells were first fixed with 4% paraformaldehyde in PBS for 10 min, washed three times with PBS, permeabilized with 0.3% Triton X-100 in PBS for 10 min, and finally saturated with PBS, 0.1% gelatin for 10 min. Cells were then incubated with commercial anti-AQP4 antibody for 30 min, washed three times with PBS, incubated for 30 min with Alexa-conjugated secondary antibodies, washed, and finally mounted in PBS/glycerol (1:1), pH 8.0, containing 1% *n*-propyl gallate. Immunostained cells were screened with a photomicroscope equipped for epifluorescence (DMRXA; Leica) and digital images were obtained with a DMX 1200 camera (Nikon, Tokyo, Japan). NMO immunostaining was performed on unfixed HeLa cells as described previously using 1:200 NMO serum (19). After incubation with secondary antibodies, the cells were fixed for 10 min with 4% paraformaldehyde.

Sample Preparation for BN-PAGE and Immunoprecipitation—A confluent layer of transfected HeLa cells was scraped and lysed into 7–10 volumes of BN-buffer (BN-buffer: 1% Triton X-100, 12 mM NaCl, 500 mM 6-aminohexanoic acid, 20 mM BisTris, pH 7.0, 2 mM EDTA, 10% glycerol) containing protease inhibitor mixture (Roche Diagnostics), vortexed on ice every 10 min for 1 h, and centrifuged at 22,000 × *g* for 30 min at 4 °C. Supernatants were collected, and the total protein content was calculated using the BCA™ protein assay kit (Pierce).

Immunoprecipitation from Transfected Cell Lysates—200 μg of proteins (see above) were incubated overnight at 4 °C on a mechanical rotator with 7 μl of anti-AQP4 commercial antibody or 1 μl of NMO or 1 μl of multiple sclerosis sera as control. The next day, 50 μl of pre-washed beads (protein G-agarose, Invitrogen) were added to the samples and incubated for an additional hour at 4 °C on a mechanical rotator. To isolate the immunocomplexes, the samples were centrifuged at 22,000 × *g* for 5 min at 4 °C; the supernatants were discarded, and the pellets were washed five times with Washing Buffer (WB: 0.2% Triton X-100, 10 mM Tris-HCl, pH 7.4, 150 mM NaCl, 1 mM EDTA, 1 mM EGTA) added with protease inhibitor mixture 1× (Roche Diagnostics), and then repeating the previous centrifugation step. The elution phase was performed adding 50 μl of Laemmli Buffer 2× without DTT (LB: 4% SDS, 20% glycerol, 0.125 mM Tris-HCl, pH 7.5, 0.004% bromphenol blue) at 60 °C for 10 min, vortexing every 5 min. After the samples were centrifuged at 13,000 rpm for 8 min. the supernatants, containing eluted proteins, were collected and analyzed by SDS-PAGE.

SDS-PAGE, BN-PAGE, and Western Blotting—5 μl of each immunoprecipitated sample were loaded onto a 12% Tris-HCl, SDS-polyacrylamide gel, and the immunoblotting step was per-

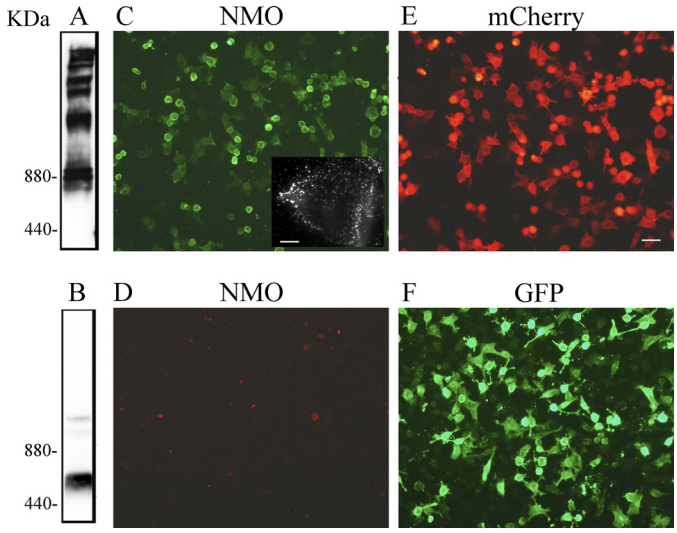

FIGURE 1. **NMO-IgG does not recognize non-OAP-forming M23-AQP4.** AQP4 immunoblot was performed after BN-PAGE using M23-mCherry (*A*) and GFP-M23 (*B*) protein extracts. Note the presence of multiple bands only in sample extracts from M23-mCherry, indicating the expression of OAPs. Representative immunofluorescence analysis of NMO-IgG binding using M23-mCherry (*C*) and GFP-M23 cells (*D*) is shown. Expression of M23-mCherry (*red, E*) and GFP-M23 (*green, F*) in transiently transfected HeLa cells is shown. *Inset* in *C* shows high magnification of a transfected cells with dot staining. *Scale bars,* 1 μm and 15 μm for the others.

formed as described. BN/SDS-PAGE was carried out as described previously (19).

Densitometric Analysis of the Immunoprecipitated AQP4—Quantification of the NMO-IgG immunoprecipitation signal was carried out by densitometric analysis with Scion Image software after normalization with WT. The values presented in the histograms are presented as mean ± S.E. of the number of experiments indicated in the figure legends. The Student's *t* test for unpaired data was employed. Differences were considered significant only when p values were <0.05.

Total Internal Reflection Fluorescence Microscopy Analysis for the Measurement of AQP4 Dots—Transfected HeLa cells were stained with commercial AQP4 as described above. The analysis of the AQP4 dots for all the mutants described in Table 1 was performed as described previously (20) using a Nikon microscope equipped for total internal reflection fluorescence.

RESULTS

NMO-IgG Does Not Recognize Non-OAP-forming AQP4-M23—To confirm previous studies that showed that NMO-IgGs recognize AQP4 assembled into OAP, we generated two fluorescent AQP4-M23 proteins tagged at the N and C termini with GFP and mCherry, respectively. Because the N terminus is important for OAP formation, addition of a fluorescent tag to the N terminus and not the C terminus of AQP4 was expected to prevent assembly into OAP. Cells expressing AQP4-M23 with an N-terminal GFP tag (GFP-M23) and AQP4-M23 with a C-terminal mCherry tag (M23-mCherry) were subjected to BN-PAGE analysis. The presence of several distinct bands, likely corresponding to AQP4-OAPs of different sizes, was found only in M23-mCherry-expressing cells (Fig. 1*A*), whereas GFP-M23 showed no significant levels of higher order structures (Fig. 1*B*), indicating that the fluorescent tag at the N terminus of AQP4-M23 affected OAP formation.

Immunofluorescence experiments showed that the NMO sera labeled M23-mCherry transfected cells (Fig. 1*C*) with a typical punctated staining (Fig. 1*C*, *inset*), but no staining was observed in the GFP-M23 cells (Fig. 1*D*). Control experiments performed on both cell lines with commercially available anti-AQP4 antibodies confirmed that the GFP-M23 expresses in the plasma membrane (data not shown). These results further confirm that NMO IgG epitope is generated by AQP4 aggregation into OAPs.

Primary Amino Acid Sequence Analysis of OAP-forming AQPs and Mutagenesis Experiments—NMO-IgG does not recognize other OAP-forming water channel proteins such as the lens AQP0 and the insect AQPcic (19, 21). To identify specific regions of AQP4 that might bind NMO-IgG, we performed an alignment analysis of AQP0 and AQPcic and human, rat, and mouse AQP4 primary amino acid sequences (Fig. 2). Extracellular loop segments were defined from previous crystallography studies (18, 22).

The alignment analysis (Fig. 2) revealed an amino acid sequence specific for AQP4 in the first extracellular loop (loop A, amino acids 60–68) between residues 61 and 64. This sequence was absent in AQP0 and in AQPcic as well as in all other human AQPs. Other differences were found within loops C (amino acids from 137 to 156) and E (amino acids from 225 to 230).

Based on the alignment results, we generated a series of rat AQP4 mutants where AQP4 specific extracellular sequences in loops A, C, and E were replaced with the corresponding sequences of AQP0 (Fig. 3 and Table 1). All these mutant channel proteins correctly targeted to the plasma membrane and formed OAPs of the same number and size of WT-AQP4 (see supplemental Fig. 1).

The 11 NMO sera and commercially available AQP4 antibodies were tested for binding by immunofluorescence and immunoprecipitation in cells transfected with these mutants. Based on the binding results, the 11 NMO sera used for this study were grouped in three sets as follows: NMO-1 (four sera), NMO-2 (five sera), and NMO-3 (two sera).

Contribution of Loop A into the NMO-IgG Epitope Formation—The contribution of the A loop in the formation of the NMO-IgG epitope was initially investigated with a mutant (Table 1 and Fig. 3) channel in which the rat AQP4-specific sequence (Gly^{61}–Asn^{64}) was deleted.

Immunofluorescence experiments (Fig. 4) showed nearly complete absence of a fluorescence signal for the NMO-1 and NMO-3 sera and a faint reduction for the NMO-2 sera. Immunoprecipitation experiments (Fig. 5, *A* and *B*, and Table 2) performed with the three classes of NMO sera, with multiple sclerosis sera and AQP4 antibodies, respectively, as negative and positive controls, confirmed the immunofluorescence results. Similar results were obtained when the human sequence Gly^{61}–Lys^{64} was deleted or when the two conserved AQP4 amino acids Gly^{61} and Glu^{63} were both mutated in lysine (data not shown). These results indicate a central role of the additional sequence in the AQP4 loop A in the NMO-binding site.

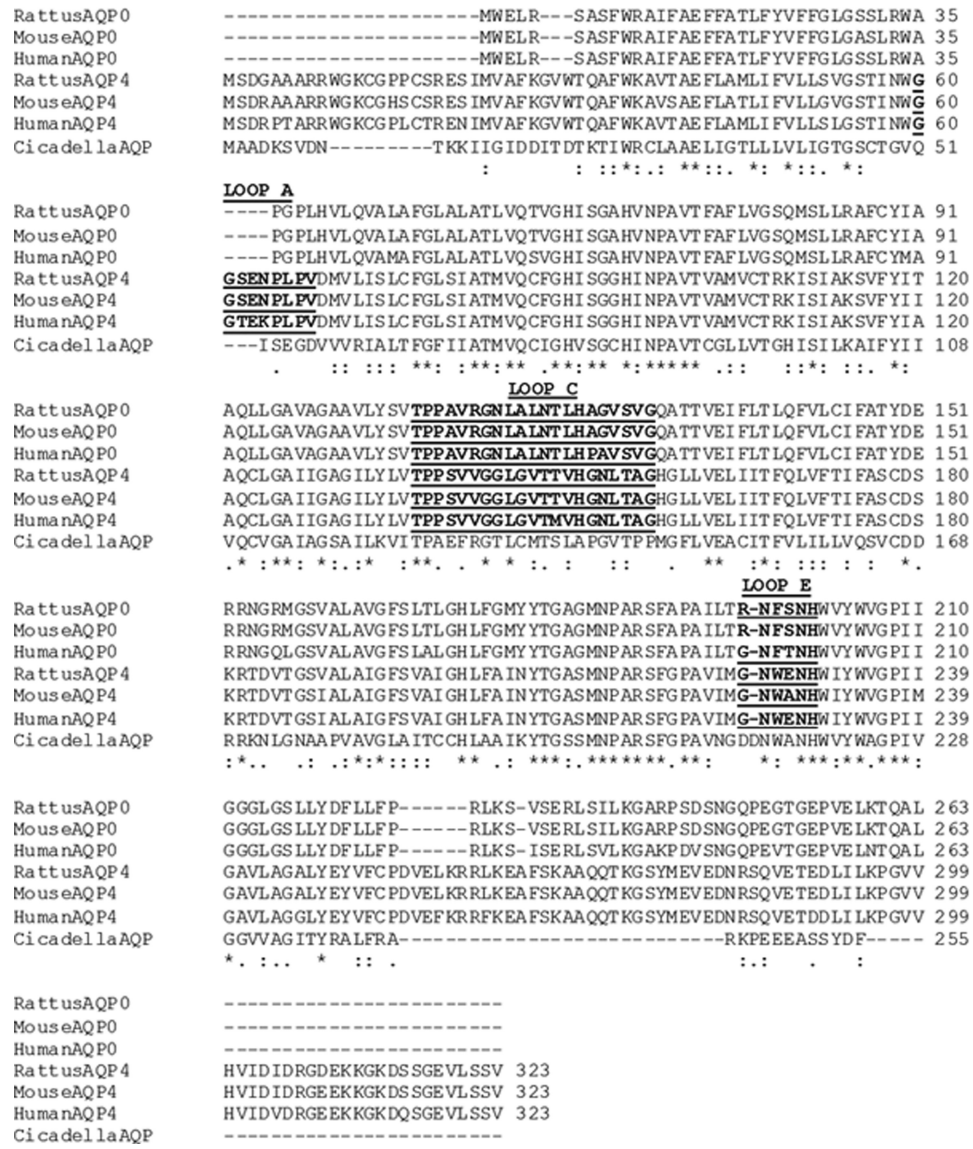

FIGURE 2**. Comparison of the primary amino acid sequence of rat, mouse, and human AQP4 and AQP0 and of *Cicadella* AQP.** Residues identical in all sequences are indicated by *asterisk*, and partially conserved amino acids are indicated by a *double* or *single dot*. The exposed extracellular loops are *highlighted*. The amino acid positions are referred to the AQP4-M1 isoform.

Contribution of C Loop and E Loop into NMO-IgG Epitope Formation—Several amino acids in the C and E loops (Fig. 2) are not conserved between AQP4 and AQP0, and these amino acids were tested as possible candidate sites for NMO-IgG binding. In the C loop, we started with the single amino acid substitutions (S140A, V142R, and G144N) in the 140–144 region, which are different than AQP4 and AQP0, and then with multiple substitutions in the 146–150 ($G^{146-150}$) and 152–157 ($G^{152-157}$) regions containing several amino acids that were also not conserved between AQP4 and AQP0 (Table 1 and Fig. 3). Immunofluorescence analysis using S140A, V142R, and G144N mutants did not show any alteration in the NMO staining (data not shown). However, a strong reduction of the staining was observed for NMO-2, and a complete absence of the staining for NMO-3 sera was found in $G^{146-150}$ mutant. No staining alteration was found for NMO-1 sera (Fig. 4). Immunoprecipitation experiments were in agreement with the immunofluorescence experiments (Fig. 5, *A* and *B,* and Table 2).

The mutant $G^{152-157}$ showed a weak reduction of the fluorescence signal for NMO-1 and NMO-3 but not for NMO-2 sera (Fig. 4). Results of immunoprecipitation experiments (Fig. 5, *A* and *B,* and Table 2) showed a significant reduction only for NMO-3 sera. The contribution of the E loop was evaluated using the mutant $W^{227-228}$. Using $W^{227-228}$, a slight reduction of fluorescence signal was observed for NMO-1 and -2, although for NMO-3 it was found to be more pronounced (Figs. 4 and 5, *A* and *B,* and Table 2). Immunoprecipitation experiments confirmed the reduction for NMO-3, although for NMO-1 and -2, it was not appreciable.

Contribution in the NMO-IgG Epitope of the Three AQP4 Extracellular Loops (A, C, and E) in Pairs by Double Mutant Analysis—Immunofluorescence analysis (Fig. 4) performed with AQP4 antibodies showed a cell membrane localization for $\Delta^{61-64}/W^{227-228}$, $G^{146-150}/W^{227-228}$, and $G^{152-157}/W^{227-228}$ mutants, whereas $\Delta^{61-64}/G^{152-157}$ and $\Delta^{61-64}/G^{146-150}/W^{227-228}$ showed an intracellular localization (data not shown). Immu-

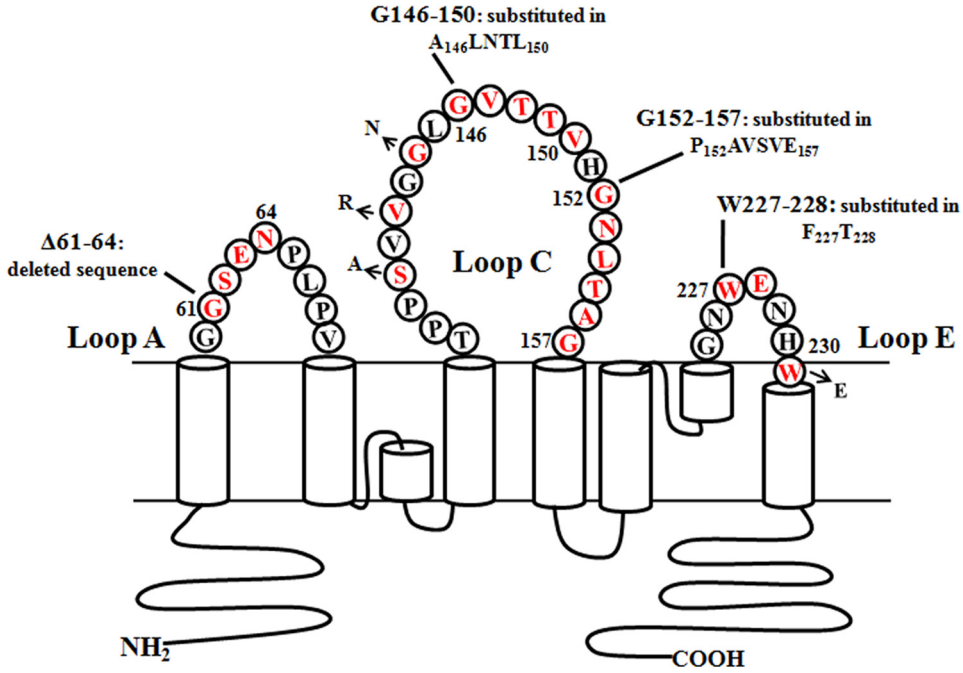

FIGURE 3. **Schematic representation of mutations performed in AQP4 extracellular loops.** Mutated amino acids, highlighted in *red,* are flanked by the mutant name and sequence. For more details see also Table 1.

TABLE 1

AQP4-M23 mutant used

Loops involved, mutant names, WT, and mutated amino acid sequences are reported. The amino acid positions refer to the AQP4-M1 isoform.

Loops	Name	WT sequence	Mutated sequence
A	Δ^{61-64}	^{61}GSEN^{64}	Absence
C	S140A	Ser^{140}	Ala^{140}
C	V142R	Val^{142}	Arg^{142}
C	G144N	Gly^{144}	Asn^{144}
C	$G^{146-150}$	^{146}GVTTV^{150}	^{146}ALNTL^{150}
C	$G^{152-157}$	^{152}GNLTAG^{157}	^{152}PAVSVE^{157}
E	$W^{227-228}$	^{227}WE^{228}	^{227}FT^{228}
A and C	$\Delta^{61-64}/G^{152-157}$	^{61}GSEN^{64}/^{152}GNLTAG^{157}	Absence + ^{152}PAVSVE^{157}
A, C, and E	$\Delta^{61-64}/G^{146-150}/W^{227-228}$	^{61}GSEN^{64}/^{146}GVTTV^{150}/^{227}WE^{228}	Absence + ^{146}ALNTL^{150} + ^{227}FT^{228}
A and E	$\Delta^{61-64}/W^{227-228}$	^{61}GSEN^{64}/^{227}WE^{228}	Absence + ^{227}FT^{228}
C and E	$G^{146-150}/W^{227-228}$	^{146}GVTTV^{150}/^{227}WE^{228}	^{146}ALNTL^{150} + ^{227}FT^{228}
C and E	$G^{152-157}/W^{227-228}$	^{152}GNLTAG^{157}/^{227}WE^{228}	^{152}PAVSVE^{157} + ^{227}FT^{228}

noprecipitation (Fig. 5, *A* and *B*, and Table 2) experiments performed with $\Delta^{61-64}/W^{227-228}$ mutant (loop A and E) show a strong reduction for NMO-1 (93 ± 1%), absence of signal for NMO-3, and a low, not statistically significant, reduction for the NMO-2 sera. Using $G^{152-157}/W^{227-228}$ (loop C and E), a similar strong immunoprecipitation reduction was obtained with NMO-1 and NMO-3 sera, although no changes were observed with NMO-2 sera (Fig. 5, *A* and *B*, and Table 2).All these results were confirmed in the corresponding immunofluorescence experiments (Fig. 4).

A significant result was obtained with the double loop mutant $G^{146-150}/W^{227-228}$; the binding of all tested sera was completely abolished. This is particularly remarkable for NMO-1 sera when we compared the results obtained with this double loop mutant with those with the single loop $G^{146-150}$ and $W^{227-228}$ mutant.

To determine whether extracellular loops of AQP4 were the only determinants to produce the NMO-IgG epitopes, we generated AQP0 mutants in which the extracellular loop amino acids were mutated to those of AQP4 (see supplemental Fig. 2, and Table 3). Mutations were sequentially produced first in loop A and then in the other loops, and NMO-Ig binding was tested in each mutant by immunofluorescence. None of the mutants, including the one that recapitulates the extracellular loops of AQP4 in AQP0, gave a clear immunofluorescence staining with NMO patient sera.

DISCUSSION

In this study, we used sera collected from Italian patients diagnosed with NMO. Eleven NMO sera were previously identified to recognize AQP4 in both brain tissue and transfected cells, and with these sera we performed this study. Using fluorescently tagged AQP4, we confirmed that the epitope was generated when AQP4-M23 organizes in OAPs. Indeed, if the fluorescent tag was added to the N terminus of M23-AQP4, the OAPs assembly was affected, and none of the 11 sera was able to bind AQP4, although if the fluorescent tag was added to the C terminus of M23-AQP4, then OAP formation was not affected, and all the sera were able to recognize AQP4. It is likely that the NMO binding involves new interactions occurring between the

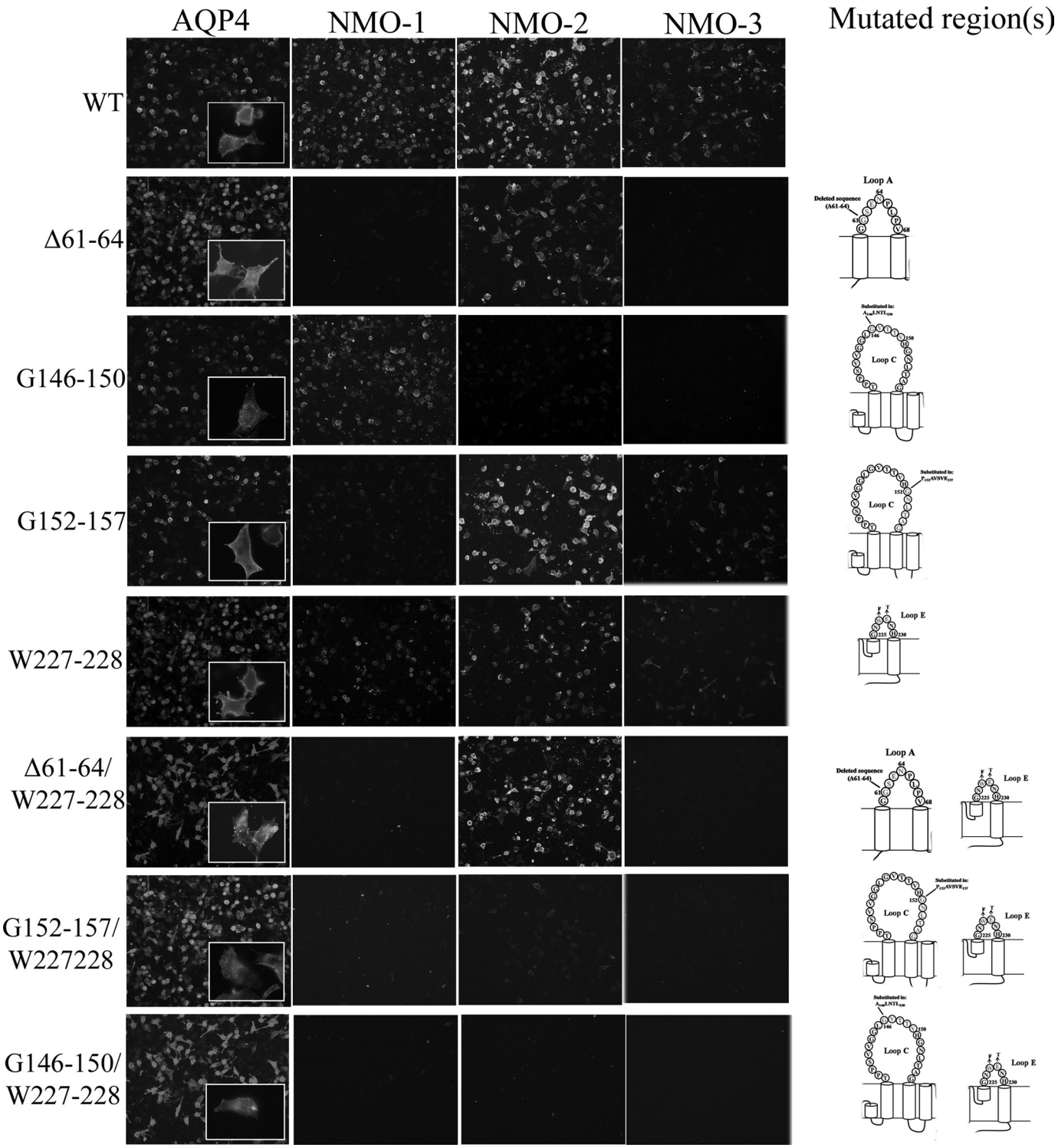

FIGURE 4. **Contribution of loop A, C, and E in the formation of NMO-IgG epitope.** Immunofluorescence experiments performed on HeLa cells transfected with mutants are reported in Table 1. Anti-AQP4 antibody (AQP4) and NMO-1, NMO-2, and NMO-3 sera are shown. *Scale bars,* 20 μm.

extracellular loops of the AQP4 tetramers when they assemble in a supramolecular organization. This suggests that OAPs formation, which occurs by lateral interaction between tetramers (22), determines new extracellular surface interactions that involve the loops A, C, and E (Fig. 6).

Here, we used mutagenesis to identify which portions of the extracellular loops were involved in binding the NMO-IgG. The study was conducted with the rat AQP4 sequence with the idea that the information obtained would be useful for the generation of a suitable animal model of the NMO. However, some results were verified using the human AQP4 mutants.

From the immunofluorescence and immunoprecipitation results, we can conclude that a group of sera (NMO-2) was able to recognize a specific portion of loop C (C_A). This

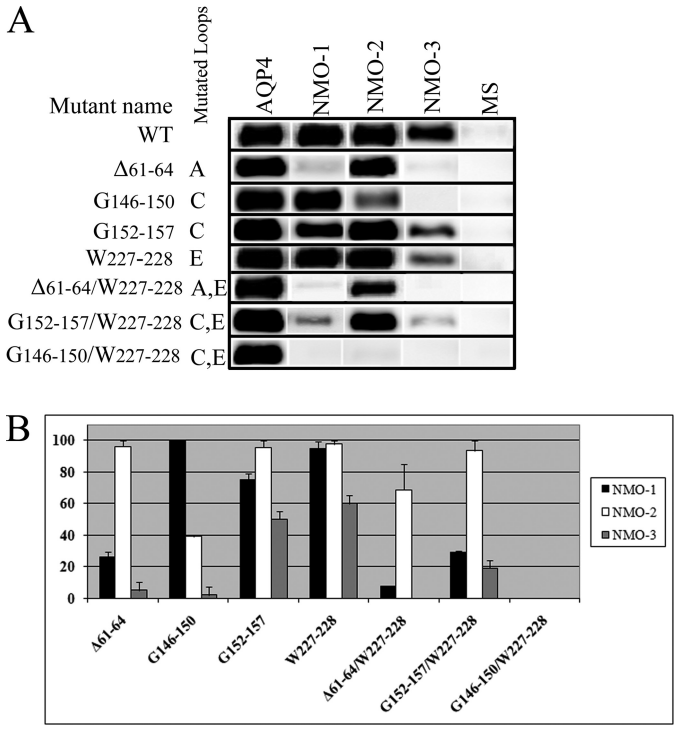

FIGURE 5. **Immunoprecipitation experiment to evaluate the loop A, C, and E contributions into the NMO-IgG epitopes.** *A,* experiment performed with NMO-1, NMO-2, and NMO-3 sera in the AQP4 mutants described previously. Immunoprecipitated proteins were revealed with anti-AQP4 commercially available antibodies. AQP4 antibodies and multiple sclerosis (*MS*) sera were used as positive and negative control, respectively. *B,* densitometric analysis of the immunoprecipitated AQP4 described in *A* ($n = 3$).

TABLE 2

The effect of mutations on the NMO-IgG binding capacity

The reduction of NMO-IgG binding capacity (% mean ± S.E.), measured by densitometric analysis of AQP4 immunoprecipitated from mutant and from WT AQP4 (Fig. 5), is shown. $n = 3$.

Loops	Mutant	NMO-1	NMO-2	NMO-3
A	Δ_{61-64}	74 ± 3^a	4 ± 3	95 ± 4^a
C	$G^{146-150}$	0	64 ± 1^a	98 ± 3^a
C	$G^{152-157}$	25 ± 4	5 ± 4	50 ± 5^b
E	$W^{227-228}$	6 ± 5	2 ± 2	40 ± 4^b
A + E	$\Delta^{61-64}/W^{227-228}$	93 ± 1^a	22 ± 15	100^a
C + E	$G^{146-150}/W^{227-228}$	100^a	100^a	100^a
C +E	$G^{152-157}/W^{227-228}$	70 ± 1^a	4 ± 6	80 ± 3^a

[a] $p < 0.001$.
[b] $p \leq 0.01$ respect to the WT.

$G^{146-150}$ region corresponds to the tip of the loop C. Because all the other mutants did not significantly affect the binding capacity of the NMO-2 group, it suggests that the NMO-2 epitope is generated by pair associations, among tetramers, of loop C (see Fig. 6).

The second group of sera (NMO-1) was characterized by a predominant role of loop A. The deletion of the four AQP4-specific amino acids (Δ^{61-64}) substantially affected the binding of this group of sera (see Table 2). However, the increased reduction in binding when the deletion of loop A is combined with loop E and the reduction found when loop C_b and loop E are mutated simultaneously suggest that the binding epitope for this group of sera is generated and/or stabilized by interaction of the extracellular loop (see Fig. 6). This epitope could be conformational as the extracellular AQP4 tetramer surface area

TABLE 3

AQP0 mutant used

Mutant names, WT, and mutated loop(s) are reported. For more details see the supplemental Fig. 2.

Name	WT loop(s)	Mutated loop(s)
WT	A, C, and E	None
Loop A	C and E	A
Loop C(a)	A, C(b), and E	C(a)
Loop C(b)	A, C(a), and E	C(b)
Loop E	A and C	E
LoopC(a + b)	A and E	C
Loop A + E	C	A and E
Loop C(a) + E	A and C(b)	C(a) and E
LoopC(b) + E	A and C(a)	C(b) and E
Loop A +C(a) + E	C(b)	A, C(a), and E
Loop A +C(b) + E	C(a)	A, C(b), and E
Loop A + C(a + b) + E	None	A, C, and E

of 35×30 Å^2 is compatible with a conformational epitope formed by the contribution of different extracellular loops (13).

The group 3, which included only two sera, was characterized by a generic reduction of the binding capacity in all the mutants that we have generated. This may be linked to the poor specificity of the sera or to an intermediate situation between group 1 and 2, but because of the scarcity of the sera, additional studies are warranted.

Two papers related to this topic have been published. Marnetto *et al.* (23), based on Western blot results, suggested that the AQP4 epitope could be linear and localized in the M1 isoform, even though this conclusion is based on the use of anti-AQP4 antibodies recognizing the C terminus of AQP4 protein, which is common between M1 and M23 isoforms. In another recent study (24), AQP4 mutants were generated based on the selective binding of the NMO sera to the human and not to the mouse form of AQP4. Using this strategy, the authors found that the major epitope of NMO-IgG is located at loop E of human AQP4. This is only partially in agreement with our results, which demonstrate that the E loop is involved with the other loops only in one category of sera. These differences may be linked to different polyclonal autoantibodies produced by Italian compared with Japanese patients or to an incomplete analysis of the complementary role of the three external loops. In support of this last possibility, the authors were not able to explain why a single amino acid substitution (A228E) in the mouse AQP4 (introducing the same amino acid of the human form) determined the recognition of their NMO sera, whereas the reciprocal human mutant E228A did not show any decrease in staining as to mouse AQP4 level. This may be explained by the involvement of other loops in the formation of the conformational epitope. Moreover, it is important to note that all our sera displayed cross-reactivity with rat and mouse AQP4.

Our data demonstrate a role of the three extracellular loops in the formation of the NMO-IgG epitope. How these loops associate and generate the epitopes for the A and B groups of sera can only be speculated at this moment. The crystal structure obtained by Ho *et al.* (18) does not provide sufficient resolution to identify amino acids involved in lateral and/or superficial interactions. From electron crystallography of double-layered, two-dimensional crystals, Hiroaki *et al.* (22) reported a superficial interaction that involves the Gly^{157} of the C loop with Trp^{231} at the end of the E loop, which generates from two adjacent tetramers that may be engaged in the NMO-

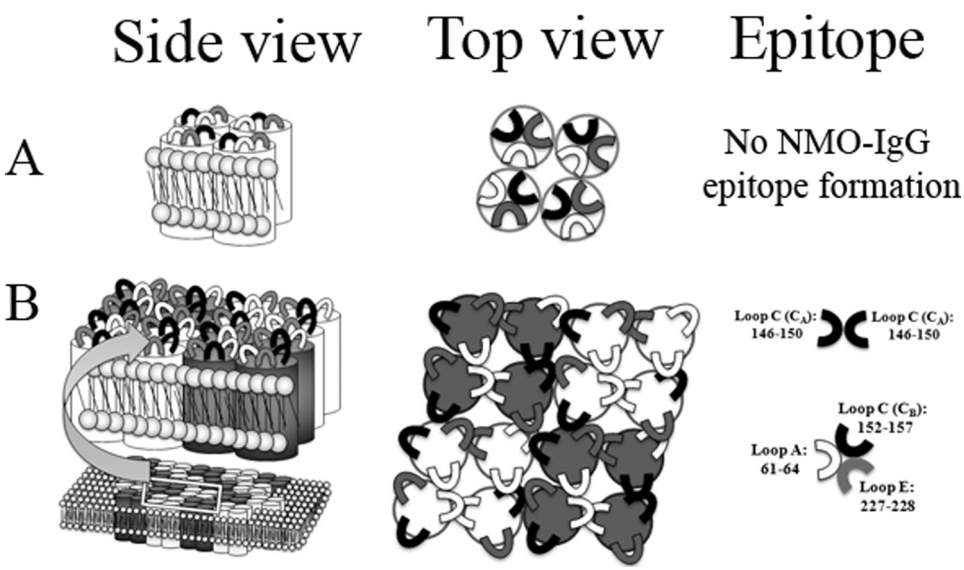

FIGURE 6. **Schematic model on how NMO epitopes could be associated to OAPs formation.** *Side* and *top views* of an AQP4 tetramer (*A*) and OAPs are shown (*B*). *A,* extracellular loops interactions in the tetramer do not generate the NMO-IgG epitope. *B,* when AQP4 organizes in OAPs, the extracellular loops of each tetramer rearrange and create at least two different NMO-IgG epitopes.

IgG epitope. We tested this hypothesis using a W231E mutant and found no effect on the interaction with the NMO sera (data not shown), indicating that this interaction is not involved in the epitope formation and, because Gly^{157} is conserved among other AQPs, probably it is not essential in the OAP formation.

To obtain additional information on the generation of these conformational epitopes, a series of AQP0 mutants was produced in which the extracellular loops were progressively mutated to make them identical to AQP4. None of the mutants was able to reproduce in AQP0 the NMO-IgG epitopes, indicating that the extracellular loops sequence *per se* is not sufficient to determine the rearrangement required to create the epitopes. One possibility to explain this result could be that the AQP0 tetramers are not sufficiently close to each other to generate OAPs of the same type as those generated by AQP4 tetramers, which are necessary to allow the interaction between loops of different tetramers. This possibility is corroborated by the analysis of two-dimensional AQP0 crystals in which the tetramers have basically no direct lateral interaction due to the presence of lipids that bridge all the contacts between tetramers (25). Furthermore, AQP4 crystallography data (22) and mutational studies (26) point to the important contribution of amino acids in the transmembrane segments and in the N terminus in the lateral interaction between tetramers necessary for AQP4-OAPs formation.

Our result provides strong evidence that the NMO-IgG epitope is not linear or within the monomer or the tetramer of AQP4. The epitope complexity could be one of the reasons why, to date, there are no NMO animal models using a linear peptide injection. Graber *et al.* (13) have recently tried to create an NMO animal model by injecting AQP4 linear peptides of the loop E (206–231) and C (272–291). These animals possessed high antibody titers able to bind the M1 and M23 isoforms, but they failed to induce any specific NMO symptoms.

The NMO-IgG epitope complexity may also explain why the disease affects some tissues but not others. Classically, NMO targets the optic nerves, the spinal cord, and to a lesser extent the brain. However, AQP4 is expressed also in other tissues such as kidney and skeletal muscle, tissues that do not appear to be affected in NMO patients. An explanation of why the primary target of NMO-IgG is the optic nerve can be related to its more permissive blood-brain barrier to serum proteins. However, it is also possible that tissue-specific structural differences in OAPs may also be involved.

In conclusion our data indicate that the NMO-IgG autoantibodies have a polyclonal origin and that the three AQP4 extracellular loops (A, C, and E) participate in the formation of the NMO-IgG epitope. These three loops likely change their conformation when AQP4 arrange into OAPs and create at least two different epitopes. The first is generated from the specific sequence present in AQP4 A loop (61–64), and the second by the involvement of the more superficial part of the C loop (C_A) of adjacent tetramers.

This study identifies key immunodominant epitopes and provides crucial information to produce an efficient NMO disease model for the development of therapy for NMO. Furthermore, we provide evidence that the transition from AQP4 tetramers to AQP4-OAPs involves conformational changes of the extracellular loops that, together with lateral interaction, may contribute to formation and/or stabilization of OAPs.

REFERENCES

1. Lennon, V. A., Wingerchuk, D. M., Kryzer, T. J., Pittock, S. J., Lucchinetti, C. F., Fujihara, K., Nakashima, I., and Weinshenker, B. G. (2004) *Lancet* **364,** 2106–2112
2. Lennon, V. A., Kryzer, T. J., Pittock, S. J., Verkman, A. S., and Hinson, S. R. (2005) *J. Exp. Med.* **202,** 473–477
3. Matsuoka, T., Matsushita, T., Kawano, Y., Osoegawa, M., Ochi, H., Ishizu, T., Minohara, M., Kikuchi, H., Mihara, F., Ohyagi, Y., and Kira, J. (2007) *Brain* **130,** 1206–1223
4. Misu, T., Fujihara, K., Kakita, A., Konno, H., Nakamura, M., Watanabe, S., Takahashi, T., Nakashima, I., Takahashi, H., and Itoyama, Y. (2007) *Brain* **130,** 1224–1234
5. Roemer, S. F., Parisi, J. E., Lennon, V. A., Benarroch, E. E., Lassmann, H.,

Bruck, W., Mandler, R. N., Weinshenker, B. G., Pittock, S. J., Wingerchuk, D. M., and Lucchinetti, C. F. (2007) *Brain* **130,** 1194–1205
6. Takahashi, T., Fujihara, K., Nakashima, I., Misu, T., Miyazawa, I., Nakamura, M., Watanabe, S., Shiga, Y., Kanaoka, C., Fujimori, J., Sato, S., and Itoyama, Y. (2007) *Brain* **130,** 1235–1243
7. Frigeri, A., Gropper, M. A., Umenishi, F., Kawashima, M., Brown, D., and Verkman, A. S. (1995) *J. Cell Sci.* **108,** 2993–3002
8. Nielsen, S., Nagelhus, E. A., Amiry-Moghaddam, M., Bourque, C., Agre, P., and Ottersen, O. P. (1997) *J. Neurosci.* **17,** 171–180
9. Pittock, S. J., Lennon, V. A., de Seze, J., Vermersch, P., Homburger, H. A., Wingerchuk, D. M., Lucchinetti, C. F., Zéphir, H., Moder, K., and Weinshenker, B. G. (2008) *Arch. Neurol.* **65,** 78–83
10. Haase, C. G., and Schmidt, S. (2001) *Neurosci. Lett.* **307,** 131–133
11. Correale, J., and Fiol, M. (2004) *Neurology* **63,** 2363–2370
12. Lalive, P. H., Menge, T., Barman, I., Cree, B. A., and Genain, C. P. (2006) *Neurology* **67,** 176–177
13. Graber, D. J., Levy, M., Kerr, D., and Wade, W. F. (2008) *J. Neuroinflammation* **5,** 22
14. Saikali, P., Cayrol, R., and Vincent, T. (2009) *Autoimmun. Rev.* **9,** 132–135
15. Hinson, S. R., McKeon, A., Fryer, J. P., Apiwattanakul, M., Lennon, V. A., and Pittock, S. J. (2009) *Arch. Neurol.* **66,** 1164–1167
16. Hinson, S. R., McKeon, A., and Lennon, V. A. (2010) *Neuroscience* **168,** 1009–1018
17. Hinson, S. R., Roemer, S. F., Lucchinetti, C. F., Fryer, J. P., Kryzer, T. J., Chamberlain, J. L., Howe, C. L., Pittock, S. J., and Lennon, V. A. (2008) *J. Exp. Med.* **205,** 2473–2481
18. Ho, J. D., Yeh, R., Sandstrom, A., Chorny, I., Harries, W. E., Robbins, R. A., Miercke, L. J., and Stroud, R. M. (2009) *Proc. Natl. Acad. Sci. U.S.A.* **106,** 7437–7442
19. Nicchia, G. P., Mastrototaro, M., Rossi, A., Pisani, F., Tortorella, C., Ruggieri, M., Lia, A., Trojano, M., Frigeri, A., and Svelto, M. (2009) *Glia* **57,** 1363–1373
20. Rossi, A., Pisani, F., Nicchia, G. P., Svelto, M., and Frigeri, A. (2010) *J. Biol. Chem.* **285,** 4562–4569
21. Le Cahérec, F., Bron, P., Verbavatz, J. M., Garret, A., Morel, G., Cavalier, A., Bonnec, G., Thomas, D., Gouranton, J., and Hubert, J. F. (1996) *J. Cell Sci.* **109,** 1285–1295
22. Hiroaki, Y., Tani, K., Kamegawa, A., Gyobu, N., Nishikawa, K., Suzuki, H., Walz, T., Sasaki, S., Mitsuoka, K., Kimura, K., Mizoguchi, A., and Fujiyoshi, Y. (2006) *J. Mol. Biol.* **355,** 628–639
23. Marnetto, F., Hellias, B., Granieri, L., Frau, J., Patanella, A. K., Nytrova, P., Sala, A., Capobianco, M., Gilli, F., and Bertolotto, A. (2009) *J. Neuroimmunol.* **217,** 74–79
24. Tani, T., Sakimura, K., Tsujita, M., Nakada, T., Tanaka, M., Nishizawa, M., and Tanaka, K. (2009) *J. Neuroimmunol.* **211,** 110–113
25. Harries, W. E., Akhavan, D., Miercke, L. J., Khademi, S., and Stroud, R. M. (2004) *Proc. Natl. Acad. Sci. U.S.A.* **101,** 14045–14050
26. Crane, J. M., Van Hoek, A. N., Skach, W. R., and Verkman, A. S. (2008) *Mol. Biol. Cell* **19,** 3369–3378